**Showcasing research from the Soft Matter Group at the Chemical Sciences Division in Oak Ridge National Laboratory, Oak Ridge, Tennessee, USA.**

Puncture-resistant self-healing polymers with multi-cycle adhesion and rapid healability

The hydrogen bonding-rich poly(dimethylsiloxane)-based elastomers in this study enable exceptional puncture-resistance, rapid self-healing, and reusable adhesion. Such design provides a new pathway for healable and puncture-resistant soft materials such as membranes and coatings with significantly improved lifetimes.
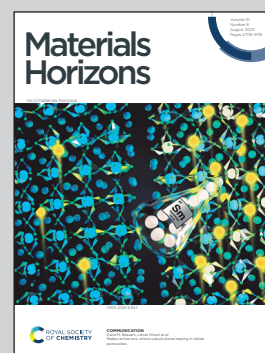
ROYAL SOCIETY OF **CHEMISTRY**

rsc.li/materials-horizons

Check for updates

Puncture-resistant self-healing polymers with multi-cycle adhesion and rapid healability†‡

Bingrui Li, [a] Sirui Ge, [c] Sheng Zhao, [b] Kunyue Xing, [b] Alexei P. Sokolov, [bd] Peng-Fei Cao [de] and Tomonori Saito [d]

The structural design of self-healing materials determines the ultimate performance of the product that can be used in a wide range of applications. Incorporating intrinsic self-healing moieties into puncture-resistant materials could significantly improve the failure resistance and product longevity, since their rapidly rebuilt bonds will provide additional recovery force to resist the external force. Herein, we present a series of tailored urea-modified poly(dimethylsiloxane)-based self-healing polymers (U-PDMS-SPs) that exhibit excellent puncture-resistant properties, fast autonomous self-healing, multi-cycle adhesion capabilities, and well-tunable mechanical properties. Controlling the composition of chemical and physical cross-links enables the U-PDMS-SPs to have an extensibility of 528% and a toughness of 0.6 MJ m^{-3}. U-PDMS-SPs exhibit fast autonomous self-healability with 25% strain recovery within 2 minutes of healing, and over 90% toughness recovery after 16 hours. We further demonstrate its puncture-resistant properties under the ASTM D5748 standard with an unbreakable feature. Furthermore, the multi-cycle adhesive properties of U-PDMS-SPs are also revealed. High puncture resistance ($>$327 mJ) and facile adhesion with rapid autonomous self-healability will have a broad impact on the design of adhesives, roofing materials, and many other functional materials with enhanced longevity.

New concepts

Puncture-resistant materials have a crucial function in personal protection devices, packaging materials, flexible electronic devices, and various other applications. Their conventional design uses strong raw materials. We here demonstrate a highly puncture-resistant and room-temperature self-healable material enabled by soft materials. The synergistic effect of hydrogen bonding and chemical cross-linking through tuning the composition during one-pot synthesis resulted in a reusable, puncture-resistant, and self-healable film and adhesive. Despite being produced from soft materials, the self-healable polymer could withhold significant puncture energy similar to tough polyurethanes. While many previous studies on self-healing materials mainly focused on the recovery of mechanical properties, this study reveals that the design of self-healing soft polymers can also benefit puncture resistance and multi-cycle adhesion. The fast molecular dynamics of the self-healing nature facilitates high puncture resistance and immediately reusable adhesion properties as well as rapid self-healability. This new design principle can be applied to the development of self-healing, puncture-resistant, and adhesive materials for many applications.

Introduction

Autonomous self-healing materials are capable of repairing physical damage without any external stimuli or intervention. This self-healing capability can be seen in living species, and human skin represents a pertinent example of a self-healing material, which can fully recover its functionalities after suffering a minor cut. Developing self-healing materials is critically important since the healing functionality is highly beneficial in various applications. One representative example is wearable electronic devices,[1,2] since these devices are constantly being operated under stretching and shrinkage with fluctuation, which may cause minor breakage. Incorporation of self-healing properties

[a] The Bredesen Center for Interdisciplinary Research and Graduate Education, University of Tennessee, Knoxville, Tennessee 37996, USA

[b] Department of Chemistry, University of Tennessee, Knoxville, Tennessee 37996, USA

[c] Department of Material Science and Engineering, University of Tennessee, Knoxville, Tennessee 37996, USA

[d] Chemical Sciences Division, Oak Ridge National Laboratory, Oak Ridge, Tennessee 37830, USA. E-mail: saitot@ornl.gov

[e] State Key Laboratory of Organic-Inorganic Composites, Beijing University of Chemical Technology, Beijing 100029, China

into materials could significantly improve the long-term performance of overall devices by extending the longevity of their functionalities.[3,4] There are two general approaches to developing self-healing materials, *i.e.*, extrinsic, and intrinsic. The extrinsic self-healing approach typically contains two isolated reactive chemicals such as dual-component epoxy with one of them being encapsulated in capsules.[5] Although this approach is simple, the design can only heal once and cannot heal the same spot repeatedly due to the irreversible nature of the healing mechanism. The intrinsic approach overcomes this shortcoming,[6] where its self-healability relies on the formation of reversible bonds that could heal repeatedly in an appropriate environment.[6,7] Intrinsic self-healing could be realized by utilizing a variety of reversible chemical bonds such as the Diels-Alder reaction,[8,9] disulfide bonds,[10,11] and boronic ester linkages,[12,13] or noncovalent reversible interactions, such as metal-ligand coordination,[14] hydrogen bonding (H-bonding),[15–18] or multiple driving forces.[19,20] Self-healable materials based on non-covalent interactions have been adopted widely over a broad range of applications including electronic devices,[21,22] coatings,[23] and functional films.[24] Compared with the self-healing materials based on dynamic covalent bonds, non-covalent interactions are normally more adaptable to self-healing in an ambient environment due to the low activation energy of bond dissociation and association.[25]

Puncture-resistant materials are typically made with woven or nonwoven fabrics. For example, puncture-resistant gloves are typically made of strong fibers like Kevlar. Their high modulus and stiffness provide high resistance to deformation while the woven texture of the fibers could distribute (or dissipate) the puncturing energy throughout the surface and further reduce the pressure at the impact point. A highly flexible and extensible material also has puncture resistance since high energy is required for puncturing such material.[26] Through the incorporation of self-healability with puncture resistance, the tolerance to damage can be further enhanced. For example, healing occurs when a puncture force is applied, and the self-healing capability could further improve the puncture-resistant properties as well as overall longevity.[26] While there have been a few reports on incorporating the self-healing concept into puncture-resistant polymeric materials,[27–30] many challenges exist, such as requiring a complicated fabrication process due to the composite structure,[29] or elevated temperature for facilitating the healing process.[28,30]

Herein, we report puncture-resistant autonomously self-healable polymers with tunable mechanical properties. The chemical and physical cross-link density of the urea-functionalized poly(dimethylsiloxane) self-healing polymer (U-PDMS-SP) is controlled by tailoring the ratio of reactants in a facile and scalable one-pot synthesis. Moreover, this U-PDMS-SP exhibits high displacement during a lap shear adhesion test and demonstrates less than 5% adhesion energy decay even after four cycle tests. Such highly puncture-resistant self-healable polymers with multi-cycle adhesion capability will have great potential for use in various applications including functional adhesives, building materials, and electronic devices.

Results and discussion

Intrinsic self-healability under ambient conditions in polymers can be achieved by the combination of reversible bonds and fast segmental dynamics. The PDMS provides one of the fastest dynamics at room temperature due to its low glass-transition temperature (T_g = −123 °C) and exhibits good chemical and thermal stability.[16] Herein, we select the commercially available amine functionalized branched PDMS (PDMS-NH$_2$-B, molecular weight = 8000 g mol^{-1}, 5 mol% amine group) and telechelic amine functionalized linear PDMS (PDMS-NH$_2$-L, molecular weight = 900 g mol^{-1}) as the main building blocks for the synthesis of self-healing polymers. As depicted in Fig. 1a, all reagents, *i.e.*, PDMS-NH$_2$-B, PDMS-NH$_2$-L, urea, and diethylenetriamine (DETA), with a controlled molar ratio were mixed without solvent and allowed to react in one pot, affording the final products at a high yield of over 85%. The single-step reaction will benefit future scale-up toward commercial adoption compared with multi-step synthesis, which is often required for synthesizing self-healing polymers.[31–35]

Urea serves as the hydrogen-bonding-containing chemical linker, and DETA is added to increase the H-bonding density in the system. The potential chemical structures of the final products are shown in Fig. S1 (ESI‡).[36] Table 1 summarizes the molar ratio of each reactant, where the cross-link density is mainly controlled by the relative ratio of PDMS-NH$_2$-B, and the H-bonding density is well-tuned by the relative ratio of DETA addition. Between U-PDMS-SP2 and U-PDMS-SP1, U-PDMS-SP1 has a higher crosslink density than U-PDMS-SP2. Similarly, U-PDMS-SP3 has a higher crosslink density than U-PDMS-SP4, while the degree of H-bonding is comparable. Since urea is the only crosslinker in the system, the only difference between U-PDMS-SP4 and U-PDMS-SP5 is that U-PDMS-SP5 has a significantly increased H-bond density compared with U-PDMS-SP4.

Four possible H-bonding units could form during this urea–amine reaction[16] as illustrated in Fig. 1a. The supramolecular interactions between the H-bonding units in U-PDMS-SPs contribute significantly to the self-healing capabilities. Since the final products are chemically cross-linked, they are insoluble in common deuterated solvents, which prevents us from using ^{1}H NMR spectroscopy for their structural analysis. As illustrated in the Fourier transform infrared (FT-IR) spectra in Fig. 1b, the normalized FT-IR absorption band corresponds to the C–Si bond at 1257 cm^{-1},[16] and the absorption bands from 3511 cm^{-1} to 3120 cm^{-1} are attributed to the N–H stretching. The significantly increased intensity of these peaks in the U-PDMS-SPs compared with those in PDMS-NH$_2$-B and PDMS-NH$_2$-L indicates the formation of urea bonds in the final product. Meanwhile, the emerging new peaks at 1561 cm^{-1} (N–H bending) and 1740–1625 cm^{-1} (C=O stretching) also indicate the formation of carbonyl bonds.[32,37] The peaks at 1632–1637 cm^{-1} (Amide I) and 1572–1574 cm^{-1} (Amide II) of U-
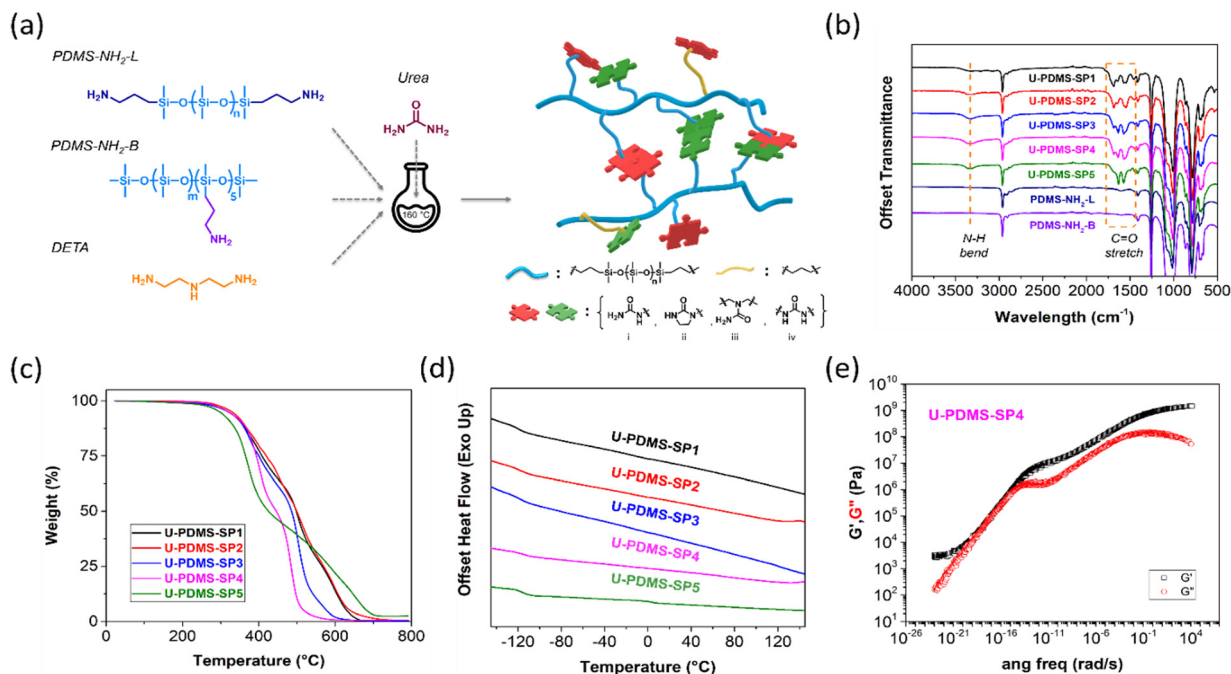
Fig. 1 (a) Schematic illustration of the chemical structures of the starting materials and the U–PDMS–SPs. (b) FT–IR spectra of U–PDMS–SPs with different ratios of reagents and PDMS starting materials after normalizing the absorption band corresponding to the C−Si bond at 1257 cm^{-1}. (c) Thermogravimetric analysis (TGA) data of U–PDMS–SPs. (d) DSC data of U–PDMS–SPs with different ratios of reagents. (e) Rheology test data curve of U–PDMS–SP4.

PDMS-SPs (Fig. S2, ESI‡) represent amide bonds in the polymer (Fig. 1a(i, iii, iv)).[38] Signals at 1687 cm^{-1} indicate the presence of an imidazolidone structure (Fig. 1a(ii)).[15] Thermogravimetric analysis (TGA) (Fig. 1c) of the U-PDMS-SPs indicates good thermal stability overall without significant weight loss below 250 °C for all the U-PDMS-SP samples (Table 1). The samples with a lower chemical cross-link density such as U-PDMS-SP4 and U-PDMS-SP5 degraded faster than other samples, which shows a notable difference in their weight losses of over 50% at 400 °C in comparison to only 25% for U-PDMS-SP1. Temperature-modulated differential scanning calorimetry (TM-DSC) was utilized to reveal the thermal properties of the U-PDMS-SPs, as seen in Fig. 1d. Only a single transition was observed in samples from U-PDMS-SP1 to U-PDMS-SP4, which corresponds to the T_g of the PDMS moiety. In addition, U-PDMS-SP5 shows another broad transition peak at ~4 °C, and this additional transition could be attributed to the phase of high –NH$_2$ group concentration that could facilitate physical cross-linking, in which a similar phenomenon is also observed in other H-bonding-rich PDMS polymers.[39] The high density of H-bonding could facilitate the

formation of physical clusters, which would require more energy to dissociate the clusters. Overall, the presence of single T_g in U-PDMS-SPs indicates that there is no significant phase separation in U-PDMS-SPs, which is also confirmed by small-angle X-ray scattering (SAXS) analysis (Fig. S3, ESI‡) in which no peaks were discovered at $q < 5$ nm^{-1} in both U-PDMS-SP4 and U-PDMS-SP5.

Rheology measurements were implemented to evaluate the viscoelastic properties of the U-PDMS-SPs. As seen in Fig. 1e and Fig. S4 (ESI‡), the U-PDMS-SPs show solid-like behavior with their storage modulus (G') higher than the loss modulus (G'') overall frequency range. The formation of numerous chemical and physical cross-links in the U-PDMS-SPs likely facilitates the transition from liquid-like starting materials to solid-like products. Comparing the G' of U-PDMS-SP1 and U-PDMS-SP2 (Fig. S4a and b, ESI‡), we observed a one-order difference at the low-frequency range. The high G' of U-PDMS-SP1 could be explained by the higher ratio of branched PDMS (PDMS-NH$_2$-B) which serves as the junction points in U-PDMS-SP1, thus, forming a higher cross-link density. Similarly, compared with U-PDMS-SP2, a higher G' is observed in

Table 1 Physical properties of U–PDMS–SPs with different compositions

Sample	PDMS-NH$_2$-B/PDMS-NH$_2$-L/Urea/DETA	$T_{d,\ 5\%}$ (°C)	T_g (°C)	Density (g cm^{-3})	G' (kPa)	Young's modulus (MPa)	Elongation-at-break (%)	Toughness (MJ m^{-3})	Ultimate tensile strength (MPa)
U-PDMS-SP1	2 : 20 : 50 : 0	319.9	−117.9	0.990 ± 0.025	42.17	0.28 ± 0.02	112.5 ± 8.7	0.12 ± 0.02	0.18 ± 0.01
U-PDMS-SP2	1 : 20 : 45 : 0	329.3	−115.8	1.031 ± 0.022	2.94	0.05 ± 0.01	411.9 ± 28.5	0.21 ± 0.03	0.10 ± 0.01
U-PDMS-SP3	1 : 20 : 105 : 20	319.9	−116.7	1.048 ± 0.004	16.65	0.18 ± 0.01	291.1 ± 16.2	0.30 ± 0.01	0.17 ± 0.01
U-PDMS-SP4	0.5 : 20 : 103 : 20	318.9	−112.4	1.060 ± 0.002	2.94	0.10 ± 0.01	528.3 ± 9.2	0.60 ± 0.02	0.21 ± 0.01
U-PDMS-SP5	0.5 : 20 : 103 : 50	297.4	−114.6	1.158 ± 0.015	—	0.02 ± 0.01	751.3 ± 30.2	0.33 ± 0.08	0.10 ± 0.02

U-PDMS-SP3. Although the PDMS-NH$_2$-B ratio is fixed, the addition of DETA introduces more H-bonding units into the U-PDMS-SP3 system. The additional H-bonding groups in U-PDMS-SP3 provide more physical interactions which afford a stronger material. In addition, by comparing U-PDMS-SP3 with U-PDMS-SP4, the lower chemical cross-link density in U-PDMS-SP4 allows a reduction of the G'. In each U-PDMS-SP sample, we observed a plateau at the lower frequency region, which could be utilized to calculate the cross-link density by the following equation:

$$c_x = \frac{2G'}{3RT} = \frac{2\rho}{3M_x}$$

where c_x is the moles of cross-links per volume, G' is the plateau value of shear modulus, R is the gas constant, T is the temperature in Kelvin, ρ is the polymer density, and M_x is the number-average molecular weight between the cross-links. As illustrated in Table 1, the U-PDMS-SP1 has a higher chemical cross-link density than U-PDMS-SP2, thus a shorter distance between crosslinks ($M_x = 5.7 \times 10^4$ g mol^{-1} for U-PDMS-SP1 versus $M_x = 8.6 \times 10^5$ g mol^{-1} for U-PDMS-SP2). U-PDMS-SP3 has more H-bonding units while having fewer chemical cross-links than U-PDMS-SP2, and the lower M_x in U-PDMS-SP3 ($M_x = 1.5 \times 10^5$ g mol^{-1}) indicates that the physical interaction (H-bonding) also contributes significantly to the overall cross-link density of the sample.

The mechanical properties of U-PDMS-SPs by tensile tests correspond well to their crosslink densities. Following the ASTM D1708 protocols, all samples were pressed at 140 °C,

and sample strips with a size of 50 mm × 5 mm × 0.3 mm were prepared. The sample strips were stretched at a rate of 1 mm s^{-1} until break, and at least three specimens were tested for accurate evaluation. As illustrated by the tensile test data shown in Fig. 2a and Table 1, the U-PDMS-SP1 exhibits high rigidity and less flexibility than U-PDMS-SP2 due to dense chemical cross-links (Table 1), which is consistent with rheology results. For example, U-PDMS-SP1 shows over 5 times higher Young's modulus (0.28 MPa versus 0.05 MPa) with a lower strain (112.5% versus 411.9%). The addition of DETA in U-PDMS-SP3 compared to U-PDMS-SP2 introduces more H-bonding-based physical cross-linking. The additional H-bonding units significantly improve Young's modulus, tensile strength, and toughness, while sacrificing 25% of the elongation-at-break. Meanwhile, consistent with the rheology result, the lack of chemical cross-links in U-PDMS-SP4 compared with U-PDMS-SP3 renders a reduced Young's modulus. The U-PDMS-SP4 exhibits the highest elongation-at-break among all the samples. The high extensibility of U-PDMS-SP4 stems from the high molecular weights of flexible PDMS chains between cross-link points (Table 1). As illustrated by the hand-pulling test in Fig. 2b, the U-PDMS-SP4 shows good extensibility, i.e., over four times its original length. Overall, the U-PDMS-SP4 exhibits the highest mechanical toughness among all the U-PDMS-SPs. Control of the density of chemical and physical cross-links can rationally tune the mechanical properties of U-PDMS-SPs, and the high toughness can be obtained by increasing the physical cross-linking while incorporating adequate chemical cross-linking. The tensile properties of U-PDMS-SPs are comparable to those of

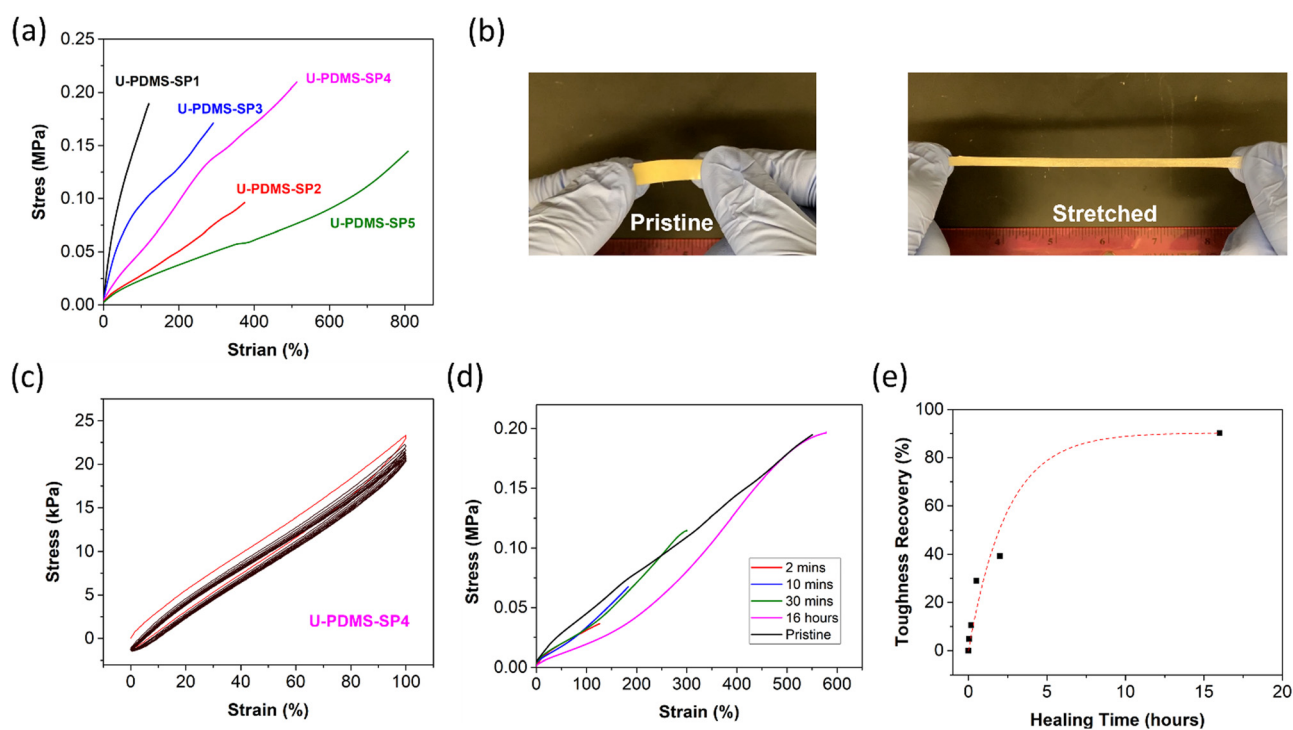
Fig. 2 (a) Tensile test data of U–PDMS–SPs at the rate of 1 mm s^{-1}. (b) Demonstration of the extensibility of U–PDMS–SP4 while the sample was stretched by hand. (c) Hysteresis test result of U–PDMS–SP4 at the rate of 1 mm s^{-1} for 10 cycles. (d) Tensile data of healed U–PDMS–SP4 at different healing times. (e) Toughness recovery percentage of U–PDMS–SP4 at different healing times.

PDMS-based elastomers.[16,40–43] Further improvement of the tensile properties could be achieved by replacing the PDMS-NH$_2$-B (5 mol% amine group) with PDMS containing a higher concentration of amine groups or incorporating other polymer matrixes or nanoparticles into U-PDMS-SPs. We also performed a hysteresis test to evaluate the elastic recovery of U-PDMS-SP4. As illustrated by the 10 cycles of hysteresis test in Fig. 2c, the U-PDMS-SP4 exhibits good elastic recovery; 95.3% of the original stress remained after the first loading–unloading cycle, which is shown as the red curve in Fig. 2c. The tensile stress loss for the following loading–unloading cycles is minimized, and the stress is maintained at 87.1% even after 10 cycles. The high elastic properties of the U-PDMS-SP4 will facilitate other functionalities, such as the puncture-resistant properties.

A supramolecular polymer network containing multiple hydrogen bonding sites with a flexible PDMS backbone exhibits exceptional self-healing potential.[16] The complex structure in the hydrogen bonding groups of U-PDMS-SPs resulted in a variety of binding energy between −16.4 and −18.2 kcal mol^{-1}.[16] Once the damaged parts were brought into physical contact, those hydrogen bonds with low binding energy at the interface could rapidly rearrange and form new bonds between the damaged parts.[15] The molecular design of U-PDMS-SPs with a high concentration of hydrogen bonding ensures sufficient hydrogen bonds could be formed rapidly to facilitate self-healing. The self-healing properties of U-PDMS-SP4 were evaluated due to its highest tensile strength and toughness among U-PDMS-SPs. Specimens of U-PDMS-SP4 were prepared with similar geometry to the tensile test samples. After cutting the specimen into two separate pieces utilizing a razor blade, those pieces were brought into contact within 30 seconds, and the re-attached polymeric specimens were healed at 20 °C for different healing times. The healed specimens were tested using the same tensile test method (customized ASTM D1708). As seen in Fig. 2d, U-PDMS-SP4 exhibits excellent room temperature self-healing properties, i.e., recovered strain value of 125% after only 2 minutes of healing from its original value of 528%. Such rapid self-healing is a synergistic effect of fast polymer dynamics from the soft PDMS backbone and the rearrangement of hydrogen bonds. After 16 hours of healing at room temperature, U-PDMS-SP4 almost fully recovered its tensile stress and extensibility. The healing dynamics were assessed by the recovery of toughness, where the recovered toughness was compared with the original toughness value (Fig. 2e). The room temperature fast healing character of U-PDMS-SP4 indicates its autonomous self-healing capability without the need for elevated temperature or prolonged time. This autonomous self-healing feature is critical for multiple applications such as smart coatings, films, sensing devices, 3D printing, etc., where repairing by active healing is not ideal during their operation.[11]

U-PDMS-SP4 further exhibits unique puncture-resistant properties during the puncture test. Following the ASTM D5748 method, the puncture resistance of the stretch wrap film was measured by the crosshead speed of 250 mm min^{-1}. Following the ASTM D5748 standard, U-PDMS-SP4 was prepared into 200 μm thickness film with a diameter of 10 cm (Fig. 3a), which covers the inner fitting of the fixture. As seen in Fig. 3d, the U-PDMS-SP4 did not break during the puncture test

since the crosshead reached its maximum travel distance. Furthermore, the sample was still maintained intact while the probe was disengaging. The energy of the puncture was estimated based on the area of the curve, although the puncture of the U-PDMS-SP4 film did not occur. The total energy to puncture is determined to be 327 mJ with a maximum force of 6.52 N at the probe travel distance of 14 cm (Fig. 3b). The high energy value is due to the high displacement that dramatically increases the overall energy value. In terms of the energy to puncture, we compared it with the state-of-the-art result of tough polyurethane, where an extremely tough polyurethane exhibits energy to puncture of 532 mJ.[44] Our soft, readily healable polymer U-PDMS-SP4 demonstrates a much higher displacement (>140 mm versus 50.6 mm) without breaking the sample, exhibiting energy to puncture of 327 mJ. The puncture energy value is expected to be much higher and most likely to be comparable to that of tough polyurethane (532 mJ),[44] since the limitation is due to the testing apparatus. The other puncture-resistant self-healing materials report 216.4 mJ (tough polyurethane)[28] and 69 mJ (soft conductive gel).[27] We also compared U-PDMS-SP4 with commercially available stretchable plastic food wrap films. U-PDMS-SP4 achieved nearly 75% of the puncture energy of the plastic food wrap film (443 mJ) while it broke early at a distance of 7 cm, which is half the distance of U-PDMS-SP4 (Fig. S5a, ESI‡). To obtain accurate values of the energy to puncture, we performed the same ASTM test on a customized sample holder with a sample diameter of 5 cm (see Fig. S5c–g, ESI‡). As seen in Fig. S5b (ESI‡), U-PDMS-SP4 was punctured after the probe reached the displacement of 14 cm (energy to puncture = 212 mJ). When compared with the food wrap film under the same testing conditions (energy to puncture = 215 mJ), the U-PDMS-SP4 demonstrated much higher displacement (140 mm versus 33 mm) and similar energy to puncture (212 mJ versus 215 mJ), although the maximum force is lower due to the reduced amount of polymer being utilized in the test. The great puncture-resistant properties of U-PDMS-SP4 are facilitated by the synergistic effect of the high extensibility of the polymer chain and rapid self-healing properties. The formation of hydrogen bonds in U-PDMS-SP4 during the puncture test enhanced the resistance of puncture, which is beyond traditional polymer chain rearrangement. When U-PDMS-SP4 is compared with hydrogen-bond-free commercial Sylgard 184 silicon elastomer (tensile strength = 5 MPa, strain = 120%)[45] for puncture-resistant properties, the U-PDMS-SP4 film absorbed 78% of the Sylgard 184's puncture energy as a much weaker polymer with only 10% of Sylgard 184's tensile toughness (Fig. S5b, ESI‡). The incorporation of self-healing properties to puncture-resistant materials could significantly improve the operating window of such materials. The improved displacement during the puncture and higher energy absorption of U-PDMS-SP4 enable its potential application for usage as puncture-resistant self-healing materials including roofing membranes, adhesive films, and flexible electronics.

Since U-PDMS-SPs possess a high concentration of H-bonds, we hypothesized that they would form H-bonds with hydroxyl-terminated surfaces and exhibit adhesive properties. We
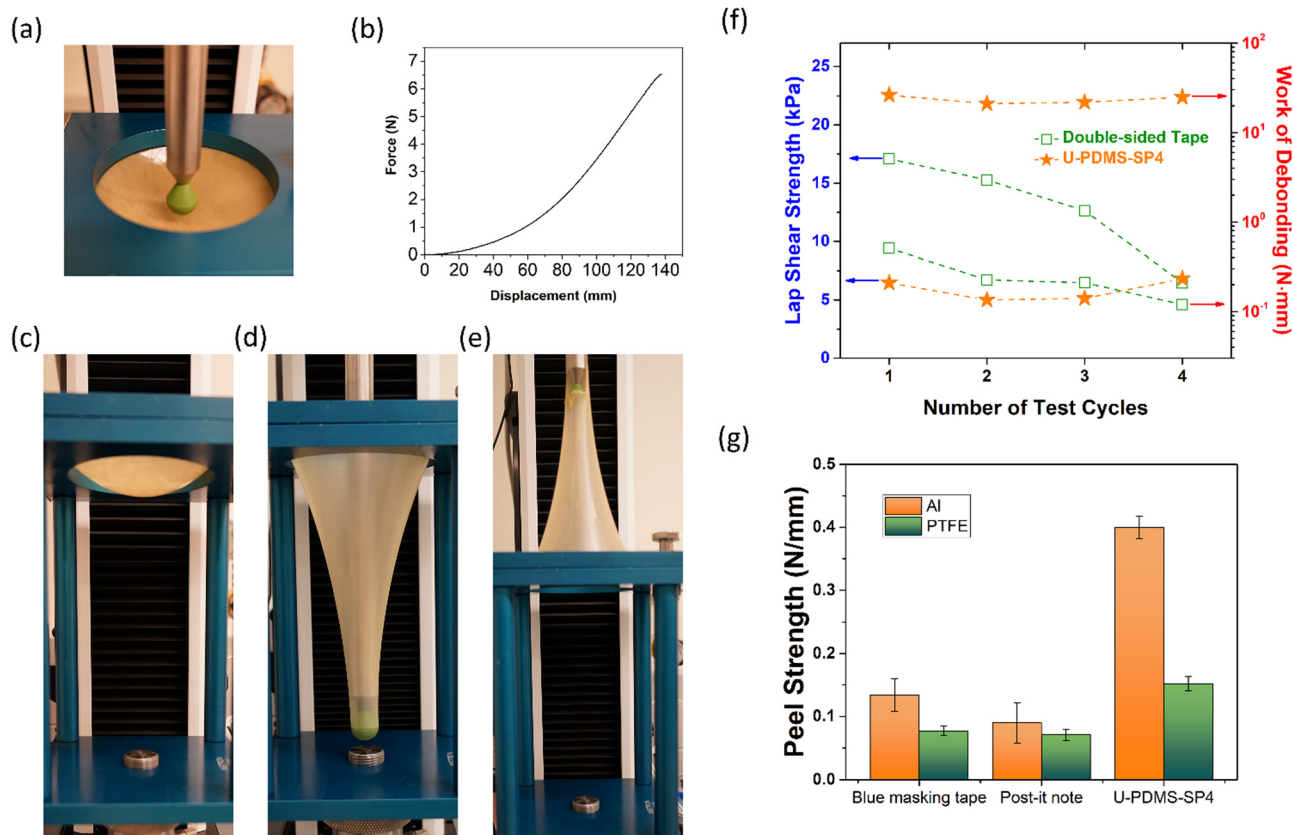
Fig. 3 (a) Pictures showing U–PDMS-SP4 being loaded on the puncture fixture, the sample diameter is 12 cm. (b) Force and displacement data during the puncture test. (c) Front view of U–PDMS-SP4 loaded on the fixture. (d) Sample punctured without breaking until the limit of the fixture. (e) Sample maintained integrity during the withdrawing of the testing rod. (f) Comparison between the lap shear strength and work of debonding data of scotch double-side tape and U–PDMS-SP4, each sample was tested four times after being reassembled within 1 minute after each test. (g) Peel test data of three different adhesives following ASTM C794 standard on aluminium (Al) and Teflon (PTFE) surfaces.

performed a lap shear adhesion test on aluminum (Al) surfaces with an overlapped surface area of (12 mm × 12 mm) 144 mm^2, following a modified version of ASTM D1002 at a rate of 2 mm min^{-1} to examine the adhesion property of U–PDMS-SP4 (Fig. S6, ESI‡). Since the U–PDMS-SP4 was exposed to an indoor atmosphere for six months before testing, the presence of dust and other particles on the polymer surface was observed.[46] For comparison, we chose commercially available scotch double-sided tape, and the same test was conducted. As seen in Fig. 3f, although the lap shear strength of U–PDMS-SP4 (6.81 kPa) is lower than that of scotch tape (17.08 kPa), the U–PDMS-SP4 exhibited a significantly higher extension (>37 mm) than the commercial double side tape (0.28 mm) (Fig. S7, ESI‡). This phenomenon is expected since the tensile strain of U–PDMS-SP4 exceeds 500%. In addition to the high extensibility, U–PDMS-SP4 was able to maintain adhesion during the extension. Fig. S8d (ESI‡) demonstrates that U–PDMS-SP4 kept holding the Al bars even after the bars were completely separated. Another intriguing adhesion characteristic of U–PDMS-SP4 is that it can be applied repeatedly while maintaining a similar level of adhesion. We performed a lap shear test four times on the same sample. The separated Al bars were put together within 1 minute after each test, and a gentle

pressure of 10–15 N was applied by hand for 1 second. Fig. 3f demonstrates the lap shear adhesion data of each cycle, then the work of debonding values was calculated. The pristine sample showed a work of debonding value of 26.3 N mm while the fourth test showed a value of 24.9 N mm. In contrast, the commercial double-side tape lost 75% of the work of the debonding value to 0.12 N mm after four tests (Fig. S7, ESI‡). The U–PDMS-SP4 demonstrates outstanding reusability while providing similar adhesion compared with commercial double-sided tape. The presence of multiple H-bonding with fast dynamics in U–PDMS-SP4 is the key characteristic facilitating fast adhesion recovery. The multi-cycle adhesive reusability through rebinding by hand pressure presents the characteristics of pressure-sensitive adhesives (PSA).

To evaluate the peel strength of U–PDMS-SP4 and compare it with other representative PSAs such as post-it notes and masking tapes, peel tests following the ASTM C794 standard on Al and polytetrafluoroethylene (PTFE) surfaces were performed (Fig. S8, ESI‡). The U–PDMS-SP4 was completely removable after the test (Fig. S8b, ESI‡). Fig. 3g shows the adhesion property comparison between the blue masking tape from 3 M, post-it notes, and U–PDMS-SP4, where their adhesion strength is 0.13, 0.09, and 0.40 N mm^{-1} on the aluminum surface, and 0.08, 0.07, and

0.15 N mm^{-1} on the PTFE surface, respectively. The self-healable adhesive, U-PDMS-SP4, exhibits 2–4 times higher peel strength on Al and PTFE surfaces than those of reusable low-force adhesives. Furthermore, the durability of U-PDMS-SP4 as PSAs is higher than that of those commercial adhesives, and we observed the smallest distributions of data between samples on U-PDMS-SP4 (Fig. 3g), which is due to its expected higher tolerance to dust, as we reported in the cases of other self-healing polymers.[47] This unique character of recoverable and high extension adhesion could be utilized for adhesives at the interfaces where there are significant movements or locations requiring multi-cycle temporal adhesion. One potential application for the U-PDMS-SPs is that it could serve as an adhesive for insulation materials such as roofing materials. With relatively low adhesion, U-PDMS-SPs could facilitate the reusing and recycling of the roofing materials, while the self-healing and puncture-resistant properties could maintain insulation after nail puncture during the installation process.

Conclusions

We developed a series of room temperature self-healable, mechanically tunable, puncture-resistant, and multi-cycle adhesive elastomers, which were successfully synthesized by scalable one-pot synthesis. Tuning the ratio of chemical and physical cross-links could tailor the mechanical properties of U-PDMS-SPs. The highly elastic U-PDMS-SP4 exhibited an elongation-at-break of over 500% and a toughness of 0.6 MJ m^{-3} with 95.3% stress remaining after a hysteresis test of 10 cycles. Although U-PDMS-SP4 is considered a "soft" polymer due to its relatively low tensile strength, its fast polymer dynamics enabled excellent room-temperature self-healing properties, exhibiting 24% of the original strain recovery after being healed for only 2 minutes. After 16 hours of healing at room temperature, 90% of the original toughness was recovered. The U-PDMS-SP4 revealed excellent puncture-resistant properties, where it exhibited the highest displacement and comparable energy to puncture values compared with different types of commercial polymer films. The U-PDMS-SP4 further exhibited high displacement and maintenance of 95% adhesion energy after four cycles of lap shear tests. These designed self-healable polymers with high tunability, high elasticity, exceptional puncture resistance, and multi-cycle adhesion provide great potential for applications such as adhesive membranes, barrier membranes, self-healable coatings, or flexible devices with significantly improved lifetimes. For example, if the U-PDMS-SP is used as a self-healable adhesive for roofing shingles, it could be deployed within a wide temperature range simply by applying pressure, and its self-healability and puncture-resistant properties will minimize the damage from nails or the other physical objects during the installation process or over the course of life. The tunable design and versatility of the self-healing polymers in this study shed light on their wide usage in various applications that require specific desirable functions such as puncture resistance or adhesion while providing a path for extended longevity of materials toward a sustainable society.

Author contributions

B. Li, P-F. Cao, and T. Saito designed the experiments and contributed to the preparation of the manuscript, B. Li, S. Ge, S. Zhao, and K. Xing performed experiments, A. P. Sokolov contributed to the discussion and revision of the manuscript.

Conflicts of interest

There are no conflicts to declare.

Acknowledgements

Notes and references

1 M. Khatib, O. Zohar and H. Haick, *Adv. Mater.*, 2021, **33**, 2004190.
2 G.-H. Zhang, L. Zhang, Q.-H. Zhu, H. Chen, W.-L. Yuan, J. Fu, S.-L. Wang, L. He and G.-H. Tao, *ACS Mater. Lett.*, 2022, **4**, 136–144.
3 C.-L. He, F.-C. Liang, L. Veeramuthu, C.-J. Cho, J.-S. Benas, Y.-R. Tzeng, Y.-L. Tseng, W.-C. Chen, A. Rwei and C.-C. Kuo, *Adv. Sci.*, 2021, **8**, 2102275.
4 J. Kang, D. Son, G.-J. N. Wang, Y. Liu, J. Lopez, Y. Kim, J. Y. Oh, T. Katsumata, J. Mun, Y. Lee, L. Jin, J. B. H. Tok and Z. Bao, *Adv. Mater.*, 2018, **30**, 1706846.
5 H. Özer, E. Kuzu, Ç. Özada, M. Ünal and M. Yazıcı, *Constr. Build. Mater.*, 2021, **310**, 125303.
6 B. Li, P.-F. Cao, T. Saito and A. P. Sokolov, *Chem. Rev.*, 2023, **123**, 701–735.
7 B. Willocq, J. Odent, P. Dubois and J.-M. Raquez, *RSC Adv.*, 2020, **10**, 13766–13782.
8 Y.-L. Liu and T.-W. Chuo, *Polym. Chem.*, 2013, **4**, 2194–2205.
9 M. B. Larsen and A. J. Boydston, *J. Am. Chem. Soc.*, 2013, **135**, 8189–8192.
10 J. Canadell, H. Goossens and B. Klumperman, *Macromolecules*, 2011, **44**, 2536–2541.
11 J. Zhu, S. Zhao, J. Luo, W. Niu, T. Damron Joshua, Z. Zhang, A. Rahman Md, A. Arnould Mark, T. Saito, R. Advincula, P. Sokolov Alexei, G. Sumpter Bobby and P.-F. Cao, *CCS Chem.*, 2022, **0**, 1–13.
12 J. J. Cash, T. Kubo, A. P. Bapat and B. S. Sumerlin, *Macromolecules*, 2015, **48**, 2098–2106.
13 Z.-H. Zhao, D.-P. Wang, J.-L. Zuo and C.-H. Li, *ACS Mater. Lett.*, 2021, **3**, 1328–1338.

14 M. Burnworth, L. Tang, J. R. Kumpfer, A. J. Duncan, F. L. Beyer, G. L. Fiore, S. J. Rowan and C. Weder, *Nature*, 2011, **472**, 334–337.

15 P. Cordier, F. Tournilhac, C. Soulié-Ziakovic and L. Leibler, *Nature*, 2008, **451**, 977–980.

16 P.-F. Cao, B. Li, T. Hong, J. Townsend, Z. Qiang, K. Xing, K. D. Vogiatzis, Y. Wang, J. W. Mays, A. P. Sokolov and T. Saito, *Adv. Funct. Mater.*, 2018, **28**, 1800741.

17 L. Zhang, Z. Liu, X. Wu, Q. Guan, S. Chen, L. Sun, Y. Guo, S. Wang, J. Song, E. M. Jeffries, C. He, F.-L. Qing, X. Bao and Z. You, *Adv. Mater.*, 2019, **31**, 1901402.

18 T. Jing, X. Heng, T. Jingqing, L. Haozhe, L. Li, L. Pingyun and G. Xiaode, *Chem. Eng. J.*, 2023, **465**, 142887.

19 L. Yang, Z. Liu, R. E. Neisiany, J. Lou, Y. Guo, L. Zhang, H. Liu, S. Chen, S. Gu and Z. You, *Sci. China: Chem.*, 2023, **66**, 853–862.

20 Q. Zhang, S. Niu, L. Wang, J. Lopez, S. Chen, Y. Cai, R. Du, Y. Liu, J.-C. Lai, L. Liu, C.-H. Li, X. Yan, C. Liu, J. B. H. Tok, X. Jia and Z. Bao, *Adv. Mater.*, 2018, **30**, 1801435.

21 J. Kang, J. B. H. Tok and Z. Bao, *Nat. Electron.*, 2019, **2**, 144–150.

22 B.-Y. Jeong, S. Lee, H. H. Shin, S. Kwon, S. H. Kim, J. H. Ryu and S. M. Yoon, *ACS Mater. Lett.*, 2022, **4**, 1944–1953.

23 Y. Li, S. Chen, M. Wu and J. Sun, *Adv. Mater.*, 2014, **26**, 3344–3348.

24 Y. Oh Jin, D. Son, T. Katsumata, Y. Lee, Y. Kim, J. Lopez, H.-C. Wu, J. Kang, J. Park, X. Gu, J. Mun, G.-J. Wang Nathan, Y. Yin, W. Cai, Y. Yun, B. H. Tok Jeffrey and Z. Bao, *Sci. Adv.*, 2019, **5**, eaav3097.

25 L. Zhang, J. Liang, C. Jiang, Z. Liu, L. Sun, S. Chen, H. Xuan, D. Lei, Q. Guan, X. Ye and Z. You, *Natl. Sci. Rev.*, 2021, **8**, nwaa154.

26 Z. Liu, L. Zhang, Q. Guan, Y. Guo, J. Lou, D. Lei, S. Wang, S. Chen, L. Sun, H. Xuan, E. M. Jeffries, C. He, F.-L. Qing and Z. You, *Adv. Funct. Mater.*, 2019, **29**, 1901058.

27 K.-X. Hou, S.-P. Zhao, D.-P. Wang, P.-C. Zhao, C.-H. Li and J.-L. Zuo, *Adv. Funct. Mater.*, 2021, **31**, 2107006.

28 X. Chen, Q. Zhong, C. Cui, L. Ma, S. Liu, Q. Zhang, Y. Wu, L. An, Y. Cheng, S. Ye, X. Chen, Z. Dong, Q. Chen and Y. Zhang, *ACS Appl. Mater. Interfaces*, 2020, **12**, 30847–30855.

29 T.-T. Li, M. Xing, B. Gao, H.-T. Ren, H.-K. Peng, X. Zhang, J.-H. Lin and C.-W. Lou, *Composites, Part A*, 2021, **145**, 106388.

30 K. Xu, G. Chen, M. Zhao, W. He, Q. Hu and Y. Pu, *RSC Adv.*, 2022, **12**, 2712–2720.

31 J. Du, Y. Li, J. Wang, C. Wang, D. Liu, G. Wang and S. Liu, *ACS Appl. Mater. Interfaces*, 2020, **12**, 26966–26972.

32 X. Wang, J. Xu, X. Zhang, Z. Yang, Y. Zhang, T. Wang and Q. Wang, *Adv. Mater.*, 2022, **34**, 2205763.

33 J. Wu, L.-H. Cai and D. A. Weitz, *Adv. Mater.*, 2017, **29**, 1702616.

34 Y. Song, Y. Liu, T. Qi and G. L. Li, *Angew. Chem., Int. Ed.*, 2018, **57**, 13838–13842.

35 D. Wan, Q. Jiang, Y. Song, J. Pan, T. Qi and G. L. Li, *ACS Appl. Polym. Mater.*, 2020, **2**, 879–886.

36 N. Guerrero-Alburquerque, S. Zhao, D. Rentsch, M. M. Koebel, M. Lattuada and W. J. Malfait, *Journal*, 2021, **13**, 1583.

37 R. Liang, H. Zhang, Y. Wang, J. Ye, L. Guo, L. He, X. Li, T. Qiu and X. Tuo, *Chem. Eng. J.*, 2022, **442**, 136204.

38 Y. Ji, X. Yang, Z. Ji, L. Zhu, N. Ma, D. Chen, X. Jia, J. Tang and Y. Cao, *ACS Omega*, 2020, **5**, 8572–8578.

39 J.-C. Lai, L. Li, D.-P. Wang, M.-H. Zhang, S.-R. Mo, X. Wang, K.-Y. Zeng, C.-H. Li, Q. Jiang, X.-Z. You and J.-L. Zuo, *Nat. Commun.*, 2018, **9**, 2725.

40 P. Wang, L. Yang, B. Dai, Z. Yang, S. Guo, G. Gao, L. Xu, M. Sun, K. Yao and J. Zhu, *Eur. Polym. J.*, 2020, **123**, 109382.

41 H. Guo, Y. Han, W. Zhao, J. Yang and L. Zhang, *Nat. Commun.*, 2020, **11**, 2037.

42 D. Döhler, J. Kang, C. B. Cooper, J. B. H. Tok, H. Rupp, W. H. Binder and Z. Bao, *ACS Appl. Polym. Mater.*, 2020, **2**, 4127–4139.

43 D.-P. Wang, Z.-H. Zhao, C.-H. Li and J.-L. Zuo, *Mater. Chem. Front.*, 2019, **3**, 1411–1421.

44 R. Guo, Q. Zhang, Y. Wu, H. Chen, Y. Liu, J. Wang, X. Duan, Q. Chen, Z. Ge and Y. Zhang, *Adv. Mater.*, 2023, 2212130.

45 I. D. Johnston, D. K. McCluskey, C. K. L. Tan and M. C. Tracey, *J. Micromech. Microeng.*, 2014, **24**, 035017.

46 A. Rahman, Md, C. Bowland, S. Ge, R. Acharya Shree, S. Kim, R. Cooper Valentino, X. C. Chen, S. Irle, P. Sokolov Alexei, A. Savara and T. Saito, *Sci. Adv.*, 2021, **7**, eabk2451.

47 Z. Zhang, N. Ghezawi, B. Li, S. Ge, S. Zhao, T. Saito, D. Hun and P.-F. Cao, *Adv. Funct. Mater.*, 2021, **31**, 2006298.